





LncRNA HAND2-AS1 promotes liver cancer stem cell self-renewal via BMP signaling

Yanying Wang^{1,†}, Pingping Zhu^{1,†}, Jianjun Luo^{2,†} , Jing Wang^{1,3,†}, Zhiwei Liu^{4,†}, Wei Wu², Ying Du¹, Buqing Ye¹, Dongpeng Wang^{2,3}, Lei He⁴, Weizheng Ren⁴, Jianyi Wang^{1,3}, Xianhui Sun^{2,3}, Runsheng Chen^{2,*} , Yong Tian^{2,3,**}  & Zusen Fan^{1,3,***} 

Abstract

Hepatocellular carcinoma (HCC) is the most prevalent liver cancer, characterized by a high rate of recurrence and heterogeneity. Liver cancer stem cells (CSCs) may well contribute to both of these pathological properties, but the mechanism underlying their self-renewal maintenance is poorly understood. Here, we identified a long noncoding RNA (lncRNA) termed HAND2-AS1 that is highly expressed in liver CSCs. Human HAND2-AS1 and its mouse ortholog *lncHand2* display a high level of conservation. HAND2-AS1 is required for the self-renewal maintenance of liver CSCs to initiate HCC development. Mechanistically, HAND2-AS1 recruits the INO80 chromatin-remodeling complex to the promoter of *BMPR1A*, thereby inducing its expression and leading to the activation of BMP signaling. Importantly, interfering with expression of HAND2-AS1 by antisense oligonucleotides (ASOs) and *BMPR1A* by siRNAs has synergistic anti-tumorigenic effects on humanized HCC models. Moreover, knockout of *lncHand2* or *Bmpr1a* in mouse hepatocytes impairs BMP signaling and suppresses the initiation of liver cancer. Our findings reveal that HAND2-AS1 promotes the self-renewal of liver CSCs and drives liver oncogenesis, offering a potential new target for HCC therapy.

Keywords BMP signaling; cancer stem cells; *HAND2-AS1*; hepatocellular carcinoma; INO80 complex

Subject Categories Cancer; RNA Biology; Stem Cells & Regenerative Medicine

DOI 10.15252/embj.2018101110 | Received 8 November 2018 | Revised 7 June 2019 | Accepted 13 June 2019 | Published online 23 July 2019

The EMBO Journal (2019) 38: e101110

Introduction

Hepatocellular carcinoma (HCC), the most common primary liver tumor, is the second leading cause of cancer death worldwide with a steady increase as a consequence of chronic hepatitis infection,

metabolic syndrome, and cirrhosis (Marquardt *et al*, 2015). In both adult and pediatric settings, treatments are inadequate, and better therapeutic targets are needed (Ji *et al*, 2009). New treatments are likely from an improved understanding of the mechanism of HCC oncogenesis. HCC is characterized by high recurrence and heterogeneity (Visvader, 2011). Heterogeneity is mainly caused by the hierarchical organization of tumor cells with a subset of cells with stem/progenitor cells known as cancer stem cells (CSCs; Meacham & Morrison, 2013). These CSCs within tumor bulk display the capacity to self-renew, differentiate, and give rise to a new tumor (Kaiser, 2015), accounting for a hierarchical organization of heterogeneous cancer cells and a high rate of recurrence. However, how liver CSCs maintain their self-renewal is unclear.

Long noncoding RNAs (lncRNAs) are a class of molecules with transcripts longer than 200 nucleotides (nt), with weak coding capacity. Compared with their protein-coding counterparts, lncRNAs are composed of fewer exons, under weaker selective constraints during evolution, and in relatively lower abundance. In addition, the expression of lncRNAs is strikingly cell and tissue specific and, in many cases, even primate specific (Fatica & Bozzoni, 2014). To date, most of the well-characterized lncRNAs have been identified. lncRNAs function in a wide range of biological processes and can regulate gene expression by diverse mechanisms (Sallam *et al*, 2016; Xing *et al*, 2017; Kopp & Mendell, 2018), including self-renewal maintenance of human liver cancer stem cells (Wang *et al*, 2015a; Zhu *et al*, 2016a,b). In cancer, lncRNAs have been reported to act as a prominent layer of transcriptional regulation (Wang *et al*, 2018b), mRNA stabilization (Hosono *et al*, 2017), often by collaborating with protein complexes. The ability of lncRNAs to control gene expression makes them potential drug targets (Matsui & Corey, 2017). Antisense oligonucleotides (ASOs) that target lncRNAs *Ube3a-ATS* (Meng *et al*, 2015) and *SAMMSON* (Leucci *et al*, 2016) showed substantial therapeutic effects on Angelman syndrome and melanoma. However, it is unknown whether lncRNAs can be used as drug candidates in liver cancer.

1 CAS Key Laboratory of Infection and Immunity, CAS Center for Excellence in Biomacromolecules, Institute of Biophysics, Chinese Academy of Sciences, Beijing, China

2 CAS Key Laboratory of RNA Biology, Institute of Biophysics, Chinese Academy of Sciences, Beijing, China

3 University of Chinese Academy of Sciences, Beijing, China

4 Department of Hepatobiliary Surgery, PLA General Hospital, Beijing, China

*Corresponding author. Tel: +86 10 6488 8543; E-mail: crs@sun5.ibp.ac.cn

**Corresponding author. Tel: +86 10 6488 8579; E-mail: ytian@ibp.ac.cn

***Corresponding author. Tel: +86 10 6488 8457; E-mail: fanz@moon.ibp.ac.cn

†These authors contributed equally to this work

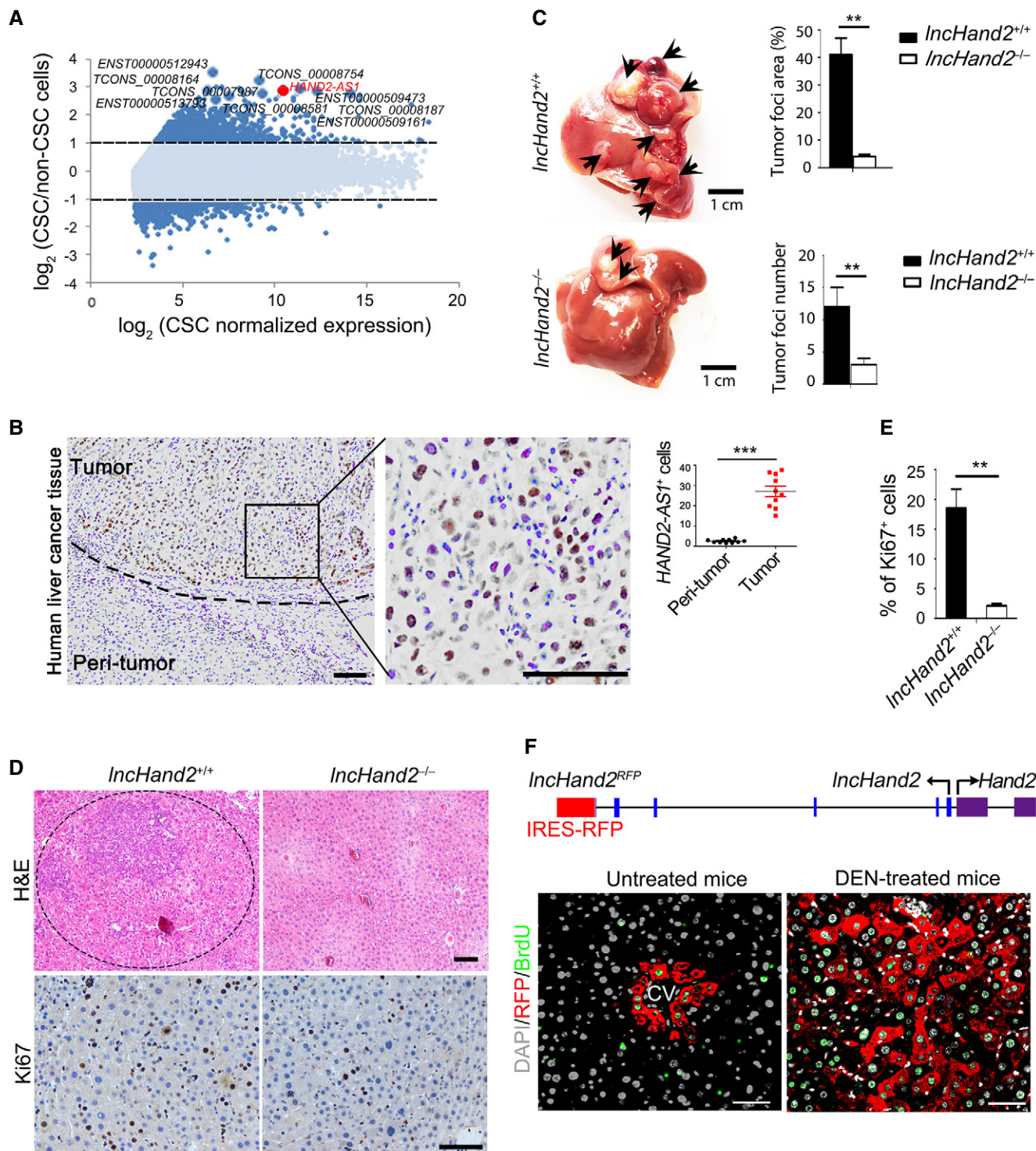


Figure 1.

The ATP-dependent chromatin-remodeling complexes have important roles in gene regulation via regulating the opening of the chromatin. The INO80 remodeling complex is a conserved complex that modifies chromatin using the energy of ATP (Ayala *et al*, 2018; Eustermann *et al*, 2018). The INO80 complex controls gene expression, DNA damage repair and replication (Krietenstein *et al*, 2016),

as well as maintaining mammalian stem cell properties (Wang *et al*, 2014). However, how it functions in liver cancer and CSCs remains unclear. Previous studies found that *HAND2-AS1* inhibits cancer migration, invasion, and metastasis (Yang *et al*, 2017, 2018). Here, we reveal that a conserved lncRNA *HAND2-AS1* is expressed at high levels in liver CSCs. *HAND2-AS1* associates with the INO80 complex

Figure 1. HAND2-AS1 is highly expressed in liver CSCs and its knockout promotes chemically induced HCC development.

- A Geometric mean-centered, hierarchical cluster heat map from microarray data. 1,077 annotated lncRNAs ($P < 0.05$) were represented in liver CSC (CD13⁺CD133⁺) compared with non-CSC (CD13⁻CD133⁻) cells sorted from three HCC primary cells of three patients. Top 10 upregulated lncRNAs in CSCs are shown.
- B *In situ* hybridization of *HAND2-AS1* in HCC tumor tissues. *HAND2-AS1* staining is shown in tumor tissues (left panel). Quantitation of *HAND2-AS1*⁺ cells in liver tissues was examined in 10 high-power fields (HPF) of sections from 10 different HCC patients (right panel). Results are shown as means \pm SEM. Scale bar, 100 μ m.
- C Macroscopic appearance of livers in 12-month-old DEN-treated *lncHand2*^{+/+} and *lncHand2* knockout (*lncHand2*^{-/-}) mice (left panel). Black arrows indicate liver tumors. Quantitation of tumor foci numbers and areas in DEN-treated livers (right panel). Results are shown as means \pm SD ($n = 12$).
- D Representative H&E and immunohistological staining with Ki67 antibody of liver sections of 12-month-old DEN-treated *lncHand2*^{+/+} and *lncHand2*^{-/-} mice. Scale bar, 100 μ m.
- E Quantitation of Ki67-positive cells in non-treated and DEN-treated mice. Bars represent average percentages and SD of cells positively staining for Ki67 cells examined in 10 HPF of sections from five different mice. Data are shown as means \pm SD.
- F Representative immunofluorescence staining of livers in 5.5-month-old DEN-treated and untreated *lncHand2*^{RFP} reporter mice for indicated molecules (lower panel). Scale bar, 100 μ m. Upper panel: scheme of targeting strategy for IRES-RFP knockin allele.
- Data information: ** $P < 0.01$ and *** $P < 0.001$ by two-tailed Student's *t*-test.

to promote BMPR1A expression and activates BMP signaling for increasing self-renewal of liver CSCs. Moreover, the addition of ASOs of *HAND2-AS1* along with siRNA against BMPR1A has potent therapeutic effect on HCC.

Results

HAND2-AS1 expression is significantly increased in liver CSCs

We sorted a small population of liver CSCs from cell lines and clinical samples with the two surface markers (CD13 and CD133; Wang et al, 2015a; Zhu et al, 2015). We showed functions of several lncRNAs in liver CSC stemness (Wang et al, 2015a; Zhu et al, 2016a,b). To further identify physiological lncRNAs involved in liver CSCs, we compared with transcriptional difference between CSCs and non-CSCs from three HCC primary tumor tissues. We found 1,077 differentially expressed lncRNA transcripts (Fig 1A), including 665 upregulated and 412 downregulated lncRNAs (Appendix Fig S1A).

We concentrated on highly conserved lncRNAs in humans and mice, which were also highly expressed in CSCs. Among these lncRNAs, we found that the knockdown of *HAND2-AS1* could significantly reduce the ability of sphere formation (Appendix Fig S1B). So we focused on a divergent lncRNA, termed as *HAND2-AS1* (gene symbol ENSG00000237125), residing on chromosome 4 in humans and on chromosome 8 in mice (termed as *lncHand2*) with the nearby gene *Hand2* (Appendix Fig S1C). *HAND2-AS1* consisted of four exons and spanning nearly 8.3-kilobase (kb), a conserved locus. We examined its level in a cohort of 50 liver tumor and paired peri-tumor tissues and eight normal tissues (Appendix Table S1). *HAND2-AS1* was highly expressed in liver tumors, whereas it was nearly undetectable in normal liver tissues by qRT-PCR analysis (Appendix Fig S1D and Table S2). Its high expression was verified in liver cancer tissues by *in situ* hybridization (Fig 1B). Furthermore, *HAND2-AS1* showed high expression in oncosphere cells (Appendix Fig S1E).

Then, we detected the transcripts of *HAND2-AS1* in liver CSCs using Northern blot. One major transcript of *HAND2-AS1* was detected, and its length was from 500 to 1,000 bases (Appendix Fig S1F). The transcript with a length of 840 nt was identified by a rapid amplification of cDNA ends (RACE) experiment (Appendix Fig S1G), with no coding potentiality using PhyloCSF (Appendix Fig

S1H) and *in vitro* translation tests (Appendix Fig S1I). Furthermore, *HAND2-AS1* mainly expressed in the nuclei of liver cancer cells via RNA fluorescence *in situ* hybridization (RNA FISH; Appendix Fig S1J) and nuclear-plasmid separation assay (Appendix Fig S1K). Thus, *HAND2-AS1* level is significantly increased in liver CSCs.

HAND2-AS1 deficiency protects against chemically induced HCC development

Given that human *HAND2-AS1* was highly conserved with mouse *lncHand2*, we previously generated *lncHand2*^{fllox/fllox} mice by a CRISPR/Cas9 approach (Wang et al, 2018a; Appendix Table S3). To investigate a potential causative relationship between *HAND2-AS1* and liver cancer development, we conditionally deleted hepatocellular *lncHand2* by crossing *lncHand2*^{fllox/fllox} mice with albumin (Alb)-Cre mice. Then, we examined chemically induced tumor formation by using diethylnitrosamine (DEN) administration in *lncHand2*^{+/+} and *lncHand2* knockout (*lncHand2*^{-/-}) mice. Macroscopic detection showed a significant decrease in numbers and volumes of tumors in *lncHand2*^{-/-} mice compared with *lncHand2*^{+/+} littermates (Fig 1C). There were few tumor areas in livers from *lncHand2*^{-/-} mice. By contrary, the livers from wild-type (WT) mice contained several large HCC tumor foci (Fig 1D). Consistent with the significantly decreased tumor areas in *lncHand2*^{-/-} mouse livers, the numbers of proliferating cells were also reduced by Ki67 staining (Fig 1D and E).

We next used *lncHand2* reporter mice as previously described and treated them with DEN for tumor induction. *lncHand2*-RFP hepatocytes mainly existed in the pericentral vein (Fig 1F). Intriguingly, *lncHand2*-RFP-positive cells diffused from the central vein to the entire liver after DEN treatment (Fig 1F). Taken together, *HAND2-AS1* promotes chemically induced liver cancer development.

HAND2-AS1 is required for liver CSCs self-renewal maintenance

For loss-of-function tests, a CRISPR/Cas9 knockout system and lentivirus-mediated short hairpin RNAs (shRNAs) against *HAND2-AS1* were performed. We used six pairs of sgRNAs and eight shRNAs to deplete *HAND2-AS1* in liver CSCs. Of these sgRNAs and shRNAs, sgRNAs (KO#1 and KO#2) and shRNAs (sh#1 and sh#2) were identified as the most robust blockers of *HAND2-AS1* expression by quantitative PCR with reverse transcription (qRT-PCR;

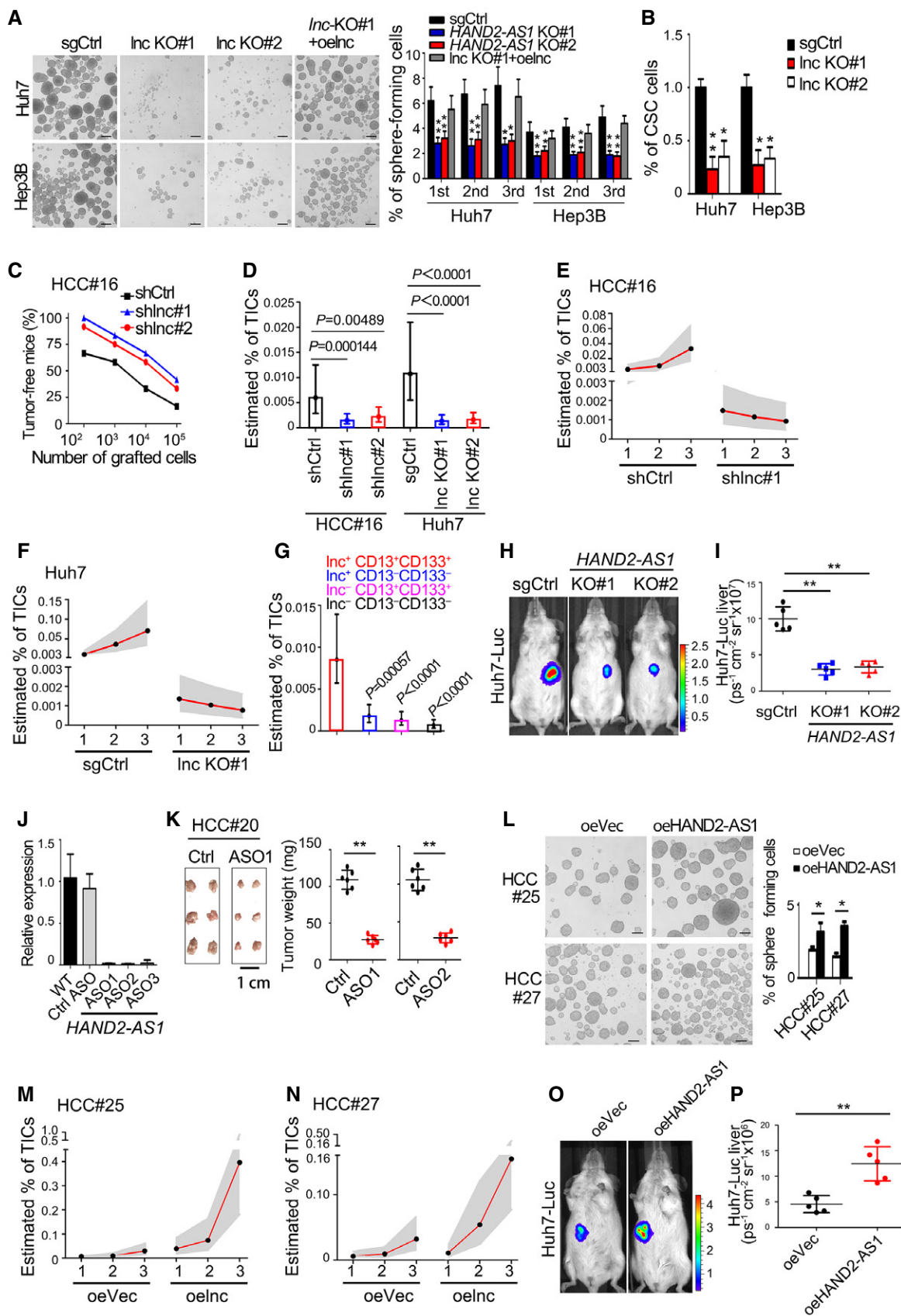


Figure 2.

Figure 2. HAND2-AS1 is required for the self-renewal maintenance of liver CSCs.

- A *HAND2-AS1* knockout causes a declined oncosphere-forming capacity in HCC cells. The right panel represents statistical results as means \pm SD ($n = 3$ per group). Overexpression of *HAND2-AS1* (oeInc) rescued the sphere formation reduced by *HAND2-AS1* deletion. Scale bar, 100 μ m.
- B CD13⁺CD133⁺ (CSC) subpopulations were detected in *HAND2-AS1* knockout cells by FACS analysis. Results are shown as means \pm SD ($n = 4$ per group).
- C Limiting diluted *HAND2-AS1* depletion or Ctrl HCC cells were subcutaneously implanted into BALB/c nude mice. $n = 12$ for each group.
- D Estimated frequency of TICs in *HAND2-AS1* deficiency and control cells after the first transplantation using the extreme limiting dilution analysis. Data are shown as the mean and 95% confidence interval. ($n = 12$ grafted tumors per dilution).
- E, F Estimated frequency of TICs in *HAND2-AS1* deficiency and control HCC cells during serial transplantations. Gray area indicates the 95% CI.
- G Estimated frequency of TICs in different populations after the first transplantation ($n = 15$ grafted tumors per dilution). Data represent the mean and 95% confidence interval.
- H Representative whole-body imaging of Huh7-Luc cells transduced with control or *HAND2-AS1* KO #1 or KO #2 vectors.
- I Quantification of tumor numbers of 6 weeks after tumor cells orthotopically implanted to B-NSG mice. Data are shown as means \pm SD. One-way ANOVA with Dunnett's correction for multiple comparisons.
- J *HAND2-AS1* expression levels (normalized to 18S rRNA) in livers from BALB/c nude mice subcutaneously transplanted xenograft primary HCC cells then intraperitoneally administered 25 mg/kg ASOs on days 15, 20, 25, 30, and 35 ($n = 5$ per group). Three ASOs (1, 2, 3) against *HAND2-AS1* were used to treat mice and showed similar depletion effects. Results are shown as means \pm SD. $n = 6$ mice per group.
- K Mice were killed at the 40th day after HCC cell injection, and the tumors were excised and weighed. Representative tumors are shown. Scale bar, 1 cm. Statistical data are shown as means \pm SD ($n = 6$ mice per group; right panel).
- L *HAND2-AS1* overexpression enhances the capacity of oncosphere formation. Scale bar, 100 μ m. oe, overexpression. Right panel: Data are shown as means \pm SD ($n = 3$ per group).
- M, N Estimated frequency of TICs in *HAND2-AS1* overexpression and control HCC cells during serial transplantations.
- O Representative whole-body imaging of Huh7-Luc cells transduced with control or *HAND2-AS1* overexpression vectors.
- P Quantification for tumor numbers 1 month after tumor cells orthotopically implanted to B-NSG mice ($n = 5$ mice per group).
- Data information: * $P < 0.05$ and ** $P < 0.01$ by two-tailed Student's *t*-test unless indicated otherwise.

Appendix Table S3, and Fig S2A and B). None of these sgRNAs or shRNAs affected intracellular levels of HAND2 and other neighboring genes (Appendix Fig S2C). Notably, *HAND2-AS1* deletion significantly declined primary (1st), secondary (2nd), and third (3rd) oncosphere formation of HCC cell lines (Fig 2A) and primary tumor cells. *HAND2-AS1* knockout significantly reduced the fraction of CD13⁺CD133⁺ cells (CSCs; Fig 2B).

The gold standard method to assess CSC potential is the extreme limiting dilutions of different cancer cell populations followed by serial tumor transplantation into immunodeficient mice to measure their ability to form secondary tumors (Boumahdi *et al*, 2014). *HAND2-AS1* deficiency impaired the ability to reform secondary tumors after transplantation (Fig 2C and D), and this difference increased in serial transplantation (Fig 2E and F). To evaluate the enrichment of tumor-initiating cells (TICs) in cells expressing CD13, CD133, and *HAND2-AS1*, we compared the ability to form secondary tumors after transplanting with the four populations (Inc⁺CD13⁺CD133⁺, Inc⁺CD13⁻CD133⁻, Inc⁻CD13⁺CD133⁺, and Inc⁻CD13⁻CD133⁻). Interestingly, Inc⁺CD13⁻CD133⁻ showed more efficient than Inc⁻CD13⁺CD133⁺ populations to reform secondary tumors ($P = 0.0368$, Fig 2G). Moreover, to assess the function of *HAND2-AS1* on orthotopic liver tumor growth, we used a CRISPR/Cas9 knockout system to transduce sgRNAs against *HAND2-AS1* into Huh7 cells containing luciferase vector (Huh7-Luc). *HAND2-AS1* deletion significantly reduced the growth of xenografts *in situ*, with remarkable inhibition of bioluminescence (Fig 2H and I, and Appendix Fig S2D). Inhibition of *HAND2-AS1* also impaired liver tumorigenesis in patient-derived xenograft (PDX) liver cancer models (Appendix Fig S2E). As a complementary acute loss-of-function approach, we used antisense oligonucleotides (ASOs) to silence *HAND2-AS1* expression. Three different ASOs effectively blocked hepatic *HAND2-AS1* expression, but not ASO scramble controls (Fig 2J), with no evidence of hepatotoxicity or Hand2 expression changes (Appendix Fig S2F). Moreover, *HAND2-AS1* ASOs administration dramatically decreased tumor growth (Fig 2K).

In addition, *HAND2-AS1* overexpression dramatically increased oncosphere formation (Fig 2L and Appendix Fig S2G), and tumor-initiating capacity using limiting dilution assays followed by serial tumor transplantation (Fig 2M and N). Consequently, *HAND2-AS1* overexpression dramatically augmented Huh7-Luc (Fig 2O and P, and Appendix Fig S2G) and liver tumorigenesis in PDX liver cancer models (Appendix Fig S2H). These data indicate that *HAND2-AS1* plays a critical role in the self-renewal maintenance of liver CSCs.

HAND2-AS1 recruits the INO80 complex and INO80 knockout suppresses liver cancer development

LncRNAs often exert their functions via RNA-interacting proteins. We thus searched for potential *HAND2-AS1* binding proteins by an RNA pulldown assay. INO80 and RUVBL2 subunits of the INO80 complex associated with *HAND2-AS1* in liver CSCs (Fig 3A, and Appendix Fig S3A and B). The INO80 complex comprises the major ATPase INO80, actin, and actin-related proteins Arp4, 5, 8 (INO80 subunits) Ies2, 4, 6, Taf14 and the AAA⁺ ATPases RUVBL1 and RUVBL2 (Eustermann *et al*, 2018). The INO80 complex can change H2A to H2A.Z as a chromatin-remodeling complex (Papamichos-Chronakis *et al*, 2011). H2A.Z, a variant of H2A, plays an important regulatory role in gene transcription (Albert *et al*, 2007). We confirmed their interaction by Western blotting (Fig 3B and Appendix Fig S3C) and RNA immunoprecipitation (RIP; Appendix Fig S3D), and by comprehensive identification of RNA binding proteins (Chu *et al*, 2015) in primary hepatocytes (Fig 3C). In contrast, *HAND2-AS1* deletion did not affect expression levels of INO80 and RUVBL2 (Appendix Fig S3E). Moreover, *HAND2-AS1* co-localized with INO80 in the nuclei of HCC oncosphere cells (Fig 3D). INO80 and RUVBL2 were highly expressed in HCC tumors (Appendix Fig S4A and B) and liver CSCs (Appendix Fig S4C). These data indicate that *HAND2-AS1* associates with the INO80 complex in the nuclei of liver CSCs.

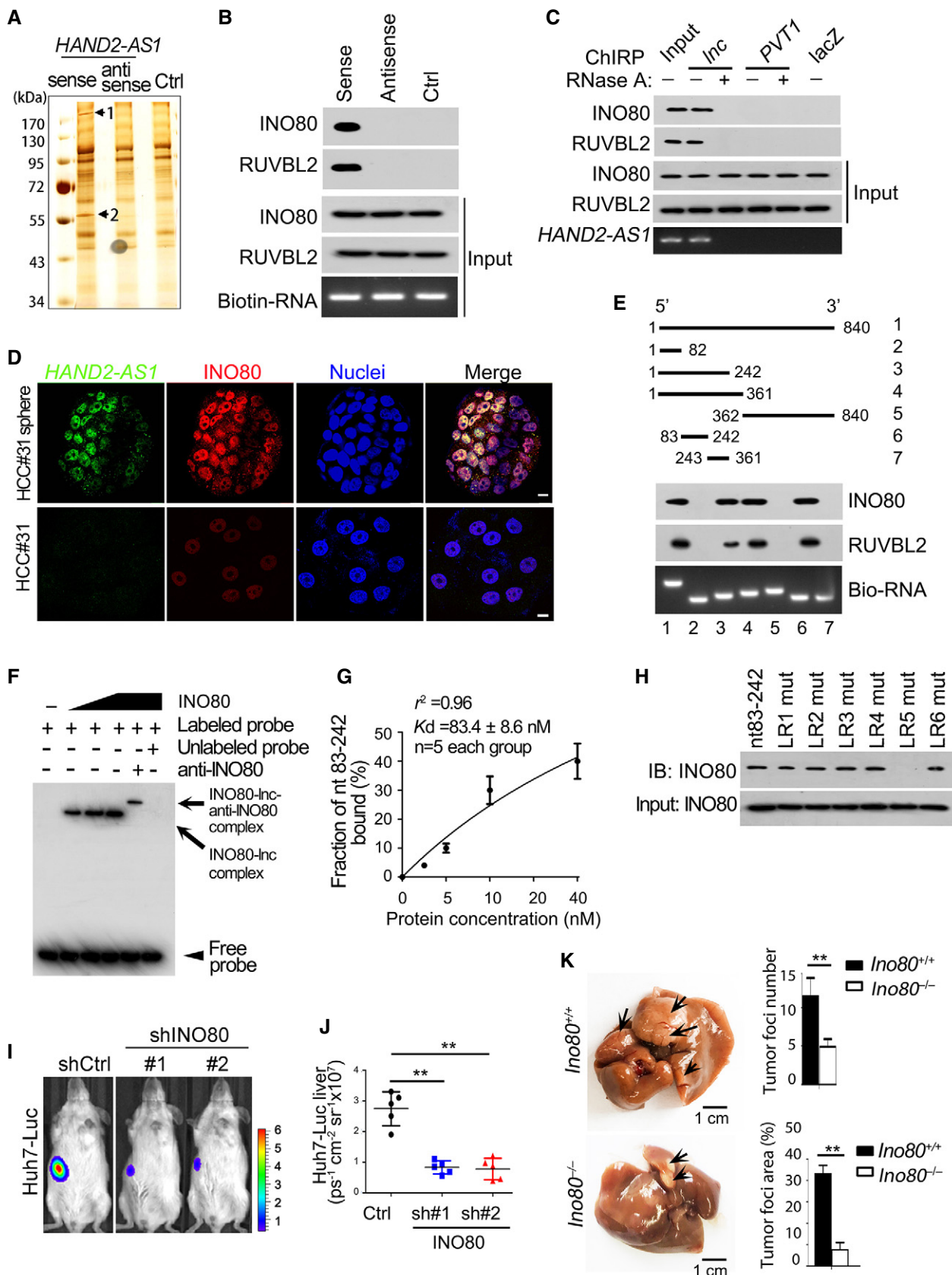


Figure 3.

Figure 3. HAND2-AS1 associates with the INO80 complex, and INO80 deficiency inhibits liver cancer development.

- A Biotin RNA pulldowns were performed with nuclear extracts of oncosphere cells using full-length *HAND2-AS1* transcript (sense), antisense, and one *HAND2-AS1* intron control, followed by mass spectrometry. Band 1: INO80, band 2: RUVBL2.
- B Two core components of the INO80 complex were confirmed by immunoblotting.
- C Immunoprecipitation assays of biotin-labeled ChIRP probes incubated with liver CSC lysates.
- D *HAND2-AS1* was visualized by RNA FISH, followed by immunofluorescence staining of INO80 in HCC primary oncosphere cells. Scale bar, 100 μ m.
- E Mapping analysis of INO80-binding domains of *HAND2-AS1*. Schematic diagram of *HAND2-AS1* full-length and truncated fragments (top panel); Western blot of INO80 and RUVBL2 in RNA pulldown samples by different *HAND2-AS1* fragments (middle panel); different *HAND2-AS1* fragments (bottom panel).
- F EMSA of biotin-labeled *HAND2-AS1* (nt 83–242) probes incubated with INO80 protein.
- G Binding affinity of *HAND2-AS1* with INO80 was determined by five independent EMSA assays. Non-linear regression curves were generated by GraphPad Prism. Results are shown as means \pm SD.
- H Interaction regions of INO80 with *HAND2-AS1* mutations at nt 83–242 of exon 2 were detected using RNA pulldown assays. LR, loop region.
- I Representative whole-body imaging of Huh7-Luc cells transduced with control or INO80 shRNA #1 or shRNA #2 vectors.
- J Quantification of tumor numbers of 4 weeks after tumor cells orthotopically implanted to B-NSG mice. Data are shown as means \pm SD ($n = 5$ mice per group). One-way ANOVA with Dunnett's correction for multiple comparisons.
- K Macroscopic appearance of livers in 10.5-month-old DEN-treated *Ino80^{fllox/fllox}* (*Ino80^{+/+}*) and *Ino80* knockout (*Ino80^{-/-}*) (left panel). Black arrows indicate tumors. Quantitation of tumor foci numbers and areas in DEN-treated livers. Results are shown as means \pm SD ($n = 10$).
- Data information: ** $P < 0.01$ by two-tailed Student's t -test.

We used a series of *HAND2-AS1* truncations to determine its binding fragment with the INO80 complex. We found that nt 83–242 of *HAND2-AS1* could bind INO80 and RUVBL2 (Fig 3E). The binding of the fragment of *HAND2-AS1* with INO80 was further confirmed by an RNA electrical mobility shift assay (EMSA; Fig 3F and G). Six loops at nt 83–242 were predicted (Appendix Fig S4D). We then mutated each loops to determine the sufficient ones for this interaction. The CTG (nt 228–230) to AAA mutation in SL5 abrogated the interaction of *HAND2-AS1* with INO80 (Fig 3H), suggesting SL5 is required for this association of *HAND2-AS1* with INO80.

To further determine the function of INO80 in liver cancer development, we depleted INO80 expression in HCC primary cells by shRNAs. Knockdown of INO80 with either of two different shRNAs decreased xenograft tumor growth (Appendix Fig S4E) and impaired self-renewal of liver CSCs (Appendix FigS4F–H). Furthermore, INO80 deficiency significantly reduced the growth of xenografts *in situ*, with remarkable inhibition of bioluminescence (Fig 3I and J). We next generated *Ino80^{fllox/fllox}* mice through insertion of *loxP* sequences flanking between the exon 2 and exon 3 of *Ino80* gene by a CRISPR/Cas9 approach (Appendix Fig S4I). We conditionally deleted *Ino80* in hepatocytes by crossing *Ino80^{fllox/fllox}* mice with Alb-Cre mice. *Ino80* was completely deleted in mouse livers (Appendix Fig S4J). We observed that *Ino80* knockout significantly decreased chemically induced liver tumor growth and numbers (Fig 3K). These data suggest that INO80 promotes liver oncogenesis and tumor development.

***HAND2-AS1* recruits the INO80 complex onto *BMPR1A* promoter to initiate its expression and BMP signaling**

To identify the targets of *HAND2-AS1*, we established *HAND2-AS1* and INO80 depleted HCC primary CSC cells and performed transcriptome microarray analysis. Of note, deficiency of *HAND2-AS1* and INO80 displayed similar transcriptome patterns (Fig 4A and Appendix Fig S5A), suggesting a functional relationship between *HAND2-AS1* and INO80. To further determine the functional role that was mediated by *HAND2-AS1*, we performed gene ontology (GO) analysis for the 2,954 genes regulated by both *HAND2-AS1* and INO80. The most implicated biological processes included

pathways in response to hypoxia, cell adhesion, cell migration, and BMP signaling (Appendix Fig S5B). Among these top enriched pathways, we wanted to focus on the pathway that was involved in the stemness regulation. The BMP signaling has been reported to be implicated in the regulation of stem cells, including hair follicle stem cells (Genander *et al*, 2014), blood stem cells (Kirmizitas *et al*, 2017), and pluripotent stem cells (Andersen *et al*, 2018). Herein, we mainly focused on the role of the BMP signaling in the modulation of liver CSCs. Integrative gene set enrichment analysis (GSEA) of the microarray data demonstrated the target genes in BMP signaling that were remarkably repressed when both *HAND2-AS1* and *INO80* were depleted (q value = 0.0003; Fig 4B), suggesting the BMP signaling was involved in the regulation of liver CSCs.

To examine genomic binding regions of *HAND2-AS1*, we performed chromatin isolation by RNA purification (ChIRP)-seq for *HAND2-AS1* in HCC tumor sphere cells and liver CSCs derived from HCC primary tumor samples. We showed *HAND2-AS1* in HCC tumor sphere cells remarkably enriched peaks compared to LacZ control (Fig 4C). After aggregating peaks from all the samples, we found 18,938 genome-wide binding sites for *HAND2-AS1* (Fig 4C). Of the 18,938 *HAND2-AS1* peaks, 8,213 bound within 1 kb of a gene transcription start site (TSS; Appendix Fig S5C). ChIRP-seq data showed that *HAND2-AS1* could bind to different loci in the genome (Fig 4D). We performed GO analysis for genes bound by *HAND2-AS1* revealed by ChIRP-seq (Appendix Fig S5D), indicating the enrichment of BMP signaling pathway. Furthermore, we analyzed ChIRP-seq genes of the BMP signaling and found *HAND2-AS1* RNA enriched at *BMPR1A*, *SMAD1*, and *SMAD9* loci (Fig 4E and Appendix Fig S5E and F). To further test how *HAND2-AS1* regulated *BMPR1A* expression, we conducted ChIRP-PCR assays with biotin-labeled *HAND2-AS1* probes. We observed that more *HAND2-AS1* transcripts were deposited on a specific region (nt –2,700 to –2,500) of the *BMPR1A* promoter than on the promoter of *SMAD1* or *SMAD9* (Fig 4F and Appendix Fig S5G–I). In addition, we isolated primary hepatocytes and carried out trimethylation of histone H3 at Lys4 (H3K4me3) assays. We noticed that this region (nt –2,700 to –2,500) of the *BMPR1A* promoter in *HAND2-AS1* knockout hepatocytes was enriched less for H3K4me3 (Appendix Fig S5J). Consequently, *HAND2-AS1* deletion caused less RNA polymerase II

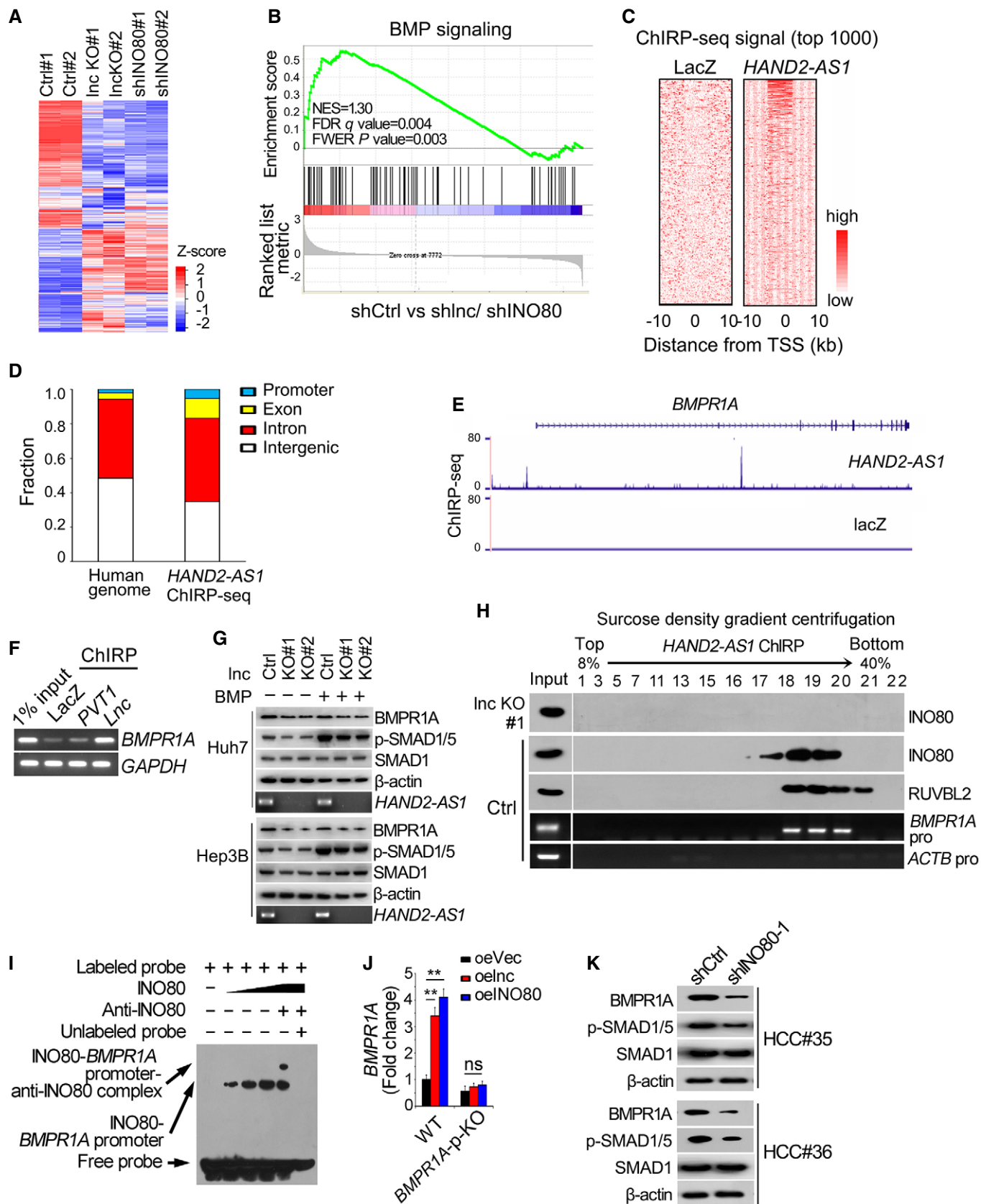


Figure 4.

Figure 4. HAND2-AS1 directly binds BMPR1A promoter to initiate its expression and activates BMP signaling.

- A Heatmap results for *HAND2-AS1* or *INO80* deficiency in HCC cells.
- B Based on GSEA results, significantly changed genes due to depletion of *HAND2-AS1* and *INO80* were attributed to the BMP signaling in HCC primary cells. NES, normalized enrichment score; FWER, familywise error rate.
- C ChIRP-seq analysis of *HAND2-AS1* genomic binding at target sites in liver CSCs, using LacZ probes as negative control. A 10-kb interval centered on the called *HAND2-AS1* peak is shown.
- D ChIRP-seq analysis of *HAND2-AS1* bound regions in the genome of liver CSCs.
- E Representative ChIRP-seq of *HAND2-AS1* binding of *BMPR1A*.
- F Gel analysis of *HAND2-AS1* RNA binding *BMPR1A* promoter in liver CSCs. LacZ and *PVT1* served as negative controls.
- G *HAND2-AS1* deletion in HCC cells decreases *BMPR1A* expression and inactivates BMP signaling.
- H ChIRP-immunoblotting analysis of *BMPR1A* interaction with the *INO80* complex in control and *HAND2-AS1*-knockout liver CSCs.
- I EMSA analysis of the interaction of *HAND2-AS1*, *INO80*, and *RUVBL2* with the *BMPR1A* promoter region.
- J *BMPR1A* promoter binding region to *HAND2-AS1/INO80* was deleted (*BMPR1A*-p-KO) in liver CSCs using lenti-Cas9, followed by *HAND2-AS1* and *INO80* overexpression (oe*HAND2-AS1*, oe*INO80*) for 36 h. *BMPR1A* mRNA levels were examined by real-time PCR. Data are shown as means \pm SD. $n = 5$. $**P < 0.01$ by two-tailed Student's *t*-test.
- K BMP signaling was examined in *INO80*-silenced liver CSCs by Western blot.

enrichment on the *BMPR1A* promoter, which was thus more resistant to DNase I digestion (Appendix Fig S5K).

In addition, *HAND2-AS1* deletion reduced *BMPR1A* expression and BMP signaling activation (Fig 4G and Appendix Fig S6A). By contrast, *HAND2-AS1* overexpression could rescue *BMPR1A* expression and BMP signaling activation (Appendix Fig S6B). In addition, *HAND2-AS1* was co-localized with p-SMAD1/5 in liver tumor tissues (Appendix Fig S6C). *HAND2-AS1* and p-SMAD1/5 were highly expressed in liver CSCs (Appendix Fig S6D). Consistent with the human liver cancer results, we found that *Bmpr1a* and BMP signaling were downregulated in liver cancer tissues from *lncHand2* knockout mice compared with *lncHand2*^{+/+} mice (Appendix Fig S6E).

Given that the *INO80* complex regulated gene transcription by binding to promoter loci and refolding chromatin, we then tested whether *HAND2-AS1* influenced *INO80* occupancy of the promoter locus of the *BMPR1A* gene. We analyzed a 3 kb locus region upstream from the TSS of the *BMPR1A* gene. We observed that *HAND2-AS1* deletion abrogated the binding capacity of *INO80* with a $-2,632$ to $-2,480$ bp segment of *BMPR1A* promoter (Appendix Fig S6F), suggesting that this segment was the binding site for *HAND2-AS1*. However, the overexpression of *HAND2-AS1* rescued this phenomenon (Appendix Fig S6G). With cross-linking treatment, *BMPR1A* was co-eluted with the *INO80* complex in WT hepatocyte lysates, but not in *HAND2-AS1* knockout hepatocyte lysates (Fig 4H). Additionally, *BMPR1A* promoter regions were also detectable in these eluates (Fig 4H). Importantly, EMSA showed that *HAND2-AS1* formed a complex with *INO80* and *BMPR1A* promoter regions (Fig 4I). Of note, *INO80* and *HAND2-AS1* overexpression did not enhance *BMPR1A* expression in *BMPR1A* promoter deleted liver cells (Fig 4J). Consistently, *INO80* deficiency dramatically suppressed BMP signaling (Fig 4K, and Appendix Fig S6H and I). Taken together, these data indicate that *HAND2-AS1* recruits the *INO80* complex onto the *BMPR1A* promoter to initiate its expression and activate BMP signaling.

BMPR1A promotes liver CSCs self-renewal via BMP signaling

To further determine the clinical implications of *BMPR1A* in HCC development, we analyzed the expression of *BMPR1A* in HCC tumor and peri-tumor tissues based on Wang's cohort (GSE14520). We observed that *BMPR1A* was highly expressed in HCC tumors

(Fig 5A), and *BMPR1A* was also an ideal prognosis predictor of liver cancers (Fig 5B). Its high expression in HCC tumor tissues was further verified by immunohistochemistry (Fig 5C). We then silenced *BMPR1A* in HCC primary cells and established stably silenced cell lines. We observed that *BMPR1A* depletion dramatically inhibited sphere formation and tumor-initiating capacity (Fig 5D and E). Moreover, *BMPR1A* depletion significantly reduced tumoral Huh7-Luc, with remarkable inhibition of bioluminescence (Fig 5F and G).

We next generated *Bmpr1a* knockout mice by CRISPR/Cas9-mediated genome editing *in vivo* (Appendix Fig S6J). We observed that *Bmpr1a* deletion reduced liver tumor formation capacity after treated with DEN compared with WT littermates (Fig 5H). Only few focal nodular hyperplastic areas were detected in histological sections of livers from DEN-treated *Bmpr1a*^{-/-} mice. In contrast, the livers of DEN-treated WT mice contained several large cancerous foci with robust proliferating cells by Ki67 staining (Fig 5I). In parallel, BMP inhibitor significantly reduced oncosphere formation (Fig 5J). By contrast, overexpression of *HAND2-AS1* or *BMPR1A* could not rescue the oncosphere-forming capacity caused by BMP inhibitor treatment (Fig 5J). Altogether, *BMPR1A* promotes liver CSC self-renewal and liver cancer development via BMP signaling pathway.

ASOs of HAND2-AS1 and siRNAs against BMPR1A have synergistic anti-tumor effects on humanized HCC models

To examine the role of *HAND2-AS1* depletion in liver cancer therapy, we used Huh7-Luc and PDX models, which recapitulated the complexity and phenotypic heterogeneity of human liver cancers (Fig 6A). PDX liver cells or Huh7-Luc cells were orthotopically transplanted into livers of NOD-*Prkdc*^{scid} *Il2rg*^{tm1}/Bcgen (B-NSG) mice. One weeks after cell injection, mice were randomly assigned to five groups to receive intraperitoneal injection of ASOs targeting *HAND2-AS1* or small interfering RNA (siRNA) that specifically targeted *BMPR1A*, or these ASOs and siRNAs together (Fig 6B). We observed that the addition of ASOs of *HAND2-AS1* or siRNAs against *BMPR1A* alone suppressed tumor growth and tumor numbers compared to vehicle-treated group (Fig 6C–F). By contrast, treatment with scramble RNAs for ASOs of *HAND2-AS1* and/or siRNAs against *BMPR1A* obtained similar results to vehicle-treated group (Fig 6C and D, and data not shown). Interestingly, the combination

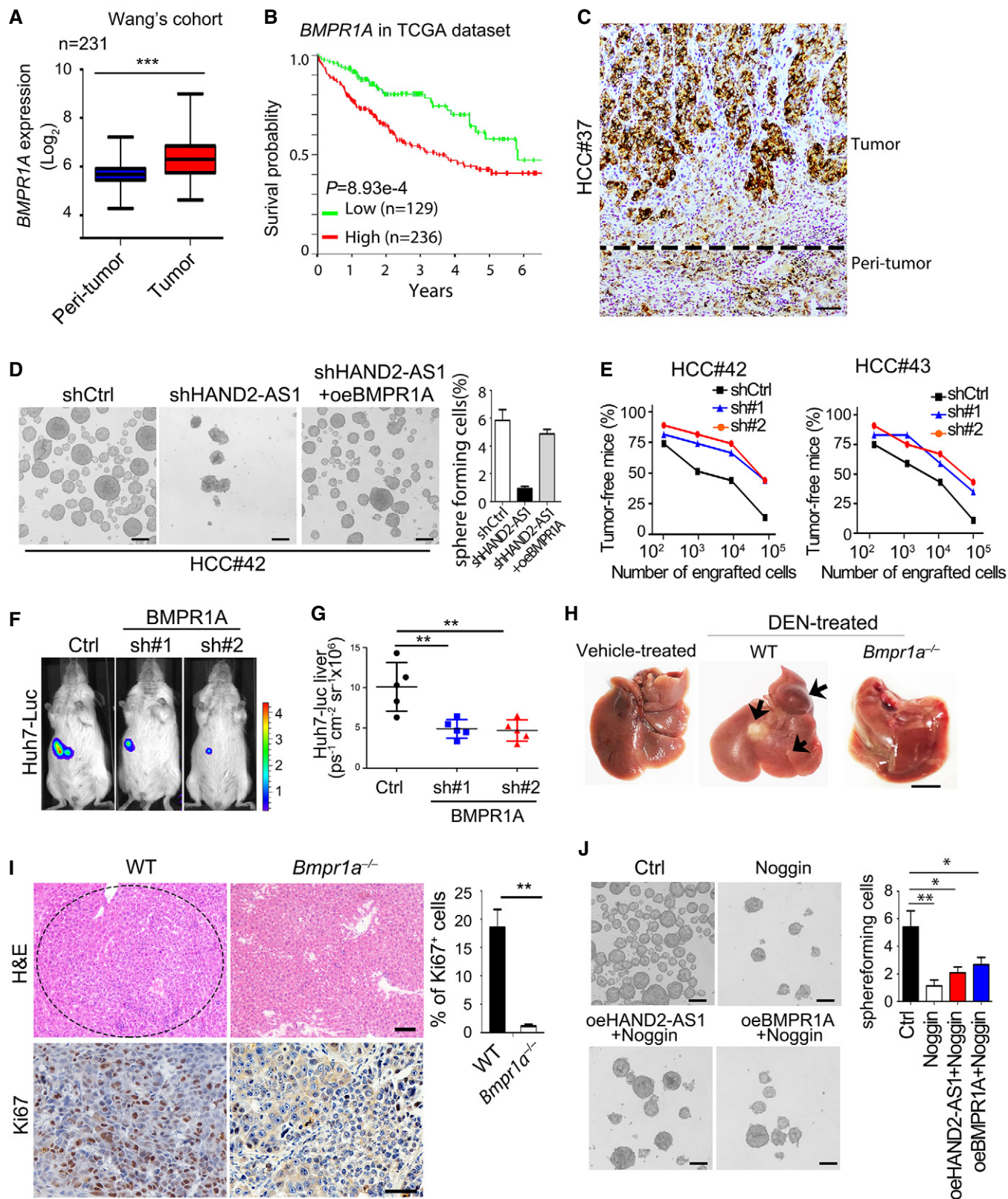


Figure 5.

Figure 5. BMPR1A promotes liver CSC self-renewal and liver cancer development.

- A BMPR1A is highly expressed in HCC tumor tissues provided by Wang's cohort (GSE14520).
- B Kaplan–Meier analyses of liver cancer outcomes in the cancer genome atlas (TCGA). *P*-value for Kaplan–Meier curves was determined using a Mantel–Cox log-rank test.
- C Representative immunohistochemistry staining of BMPR1A was detected in HCC samples. Scale bar, 100 μ m.
- D BMPR1A overexpression rescues sphere formation ability reduced by *HAND2-AS1* depletion in HCC samples. Representative sphere formation is shown on the left panel. Scale bar, 100 μ m. Percentages of sphere-forming cells were calculated as means \pm SD (right panel). *n* = 4.
- E *BMPR1A* depletion reduces tumor-initiating capacity. *n* = 12 mice per group.
- F Representative whole-body imaging of Huh7-Luc cells transduced with scramble (Ctrl) or *BMPR1A* shRNAs.
- G Quantification for tumor numbers of 7 weeks after tumor cells orthotopically implanted to B-NSG mice. Calculated data are shown as means \pm SD (*n* = 5 mice per group).
- H Macroscopic appearance of livers from 10-month-old mice treated by DEN or vehicle. Scale bar, 1 cm. Black arrows indicate tumors.
- I Representative H&E and immunohistological staining with Ki67 antibody in liver sections of 10-month-old DEN-treated WT and *Bmpr1a*^{-/-} mice. Scale bar, 100 μ m. Right: Quantitation of Ki67-positive cells in DEN-treated mice. Data are shown as means \pm SD. *n* = 5.
- J BMP signaling inhibitor noggin decreased tumor sphere formation. Scale bar, 100 μ m. Right: Data are shown as means \pm SD (*n* = 4).
- Data information: **P* < 0.05, ***P* < 0.01, and ****P* < 0.001 by two-tailed Student's *t*-test unless indicated otherwise.

of *HAND2-AS1* ASOs and BMPR1A siRNAs displayed synergistic therapeutic effects on humanized HCC models (Fig 6C–F). As expected, administration of *HAND2-AS1* ASOs and BMPR1A siRNAs remarkably inhibited cell proliferation of xenografts (Fig 6G) as well as expression of *HAND2-AS1* and BMPR1A (Fig 6H). Consequently, treatment with *HAND2-AS1* ASOs and BMPR1A siRNAs prolonged survival rates compared to that of vehicle-treated group (Fig 6I and J). Collectively, targeting *HAND2-AS1* and BMPR1A has synergistic anti-tumor effects on humanized HCC models.

Discussion

lncRNAs play widespread roles in many cellular processes via various mechanisms (Batista & Chang, 2013; Ulitsky & Bartel, 2013; Flynn & Chang, 2014). We previously sorted liver CSCs with the combination of CD13 and CD133 and defined several lncRNAs from liver CSCs of HCC cell lines that play important roles in the regulation of liver CSC stemness (Wang et al, 2015a; Zhu et al, 2015). Here, we identified physiological lncRNAs in liver CSCs from HCC primary samples. Of these high expressed lncRNAs in liver CSCs, we focused on *HAND2-AS1* that was a divergent lncRNA against the *HAND2* gene. *HAND2-AS1* is highly conserved in humans and mice. *HAND2-AS1* is highly expressed in liver CSCs and is required for the self-renewal maintenance of liver CSCs. Mechanically, *HAND2-AS1* recruits the INO80 complex onto BMPR1A promoter to initiate its expression, leading to the activation of BMP signaling. Importantly, targeting *HAND2-AS1* and BMPR1A has synergistic anti-tumor effects on humanized HCC models. Our findings indicate that lncRNAs play critical roles in the maintenance regulation of liver CSCs and may serve as potential targets for cancer therapy.

Divergent lncRNAs are transcribed in the opposite direction to their nearby protein-coding genes (Lau, 2014). Compared with 75% of lncRNAs showing a *cis*-regulatory effect, only 20–25% of divergent noncoding/coding genes appear to have effects on nearby transcription upon deficiency, which suggests context-dependent lncRNA regulation (Luo et al, 2016; Kopp & Mendell, 2018). lncRNA/coding gene pairs showed significantly higher expression correlation than coding/coding gene pairs. For instance, lncRNA *Fendrr* deficiency specifically reduces levels of its divergent nearby

gene *FOXF1*, but not other neighboring genes. Knockdown of divergent lncRNA *Evx1as* transcripts without altering genomic sequences led to downregulation of *EVX1* during mesendodermal differentiation. However, in embryonic stem cells (ESCs), *Evx1as* might have roles beyond controlling *EVX1* expression (Luo et al, 2016). Depletion of *HAND2-AS1* transcripts by loss-of-function approaches in HCC cells, including CRISPR, RNAi, and ASOs, does not affect expression levels of its divergent protein-coding gene *HAND2* and other nearby genes. On the other hand, *lncHand2* knockout does not affect the expression of *Hand2* and other neighboring genes in mouse livers. In addition, transcriptomic analysis of *HAND2-AS1* deletion and ChIRP-seq of *HAND2-AS1* does not display additional genomic effects on *HAND2* and other nearby genes, ruling out its *cis* function. We conclude that *HAND2-AS1* modulates the self-renewal maintenance of liver CSCs in *trans*.

Since most of lncRNAs are lack of evolutionary conservation in humans and mice (Matsui & Corey, 2017), it is difficult to explore their physiological roles and test their therapeutic effects with animal models. We aimed to identify critically evolutionary conservative lncRNAs in liver CSCs and reveal their real roles in the pathogenesis and therapeutic targets of liver cancer. As this criterion, *HAND2-AS1* was highly conserved in various species, including humans and mice. Its mouse ortholog is *lncHand2*, a divergent lncRNA for murine *Hand2* gene. We observed that *Hand2* deletion causes early embryonic lethality. *HAND2* deletion in HCC tumor cells does not affect cell growth and self-renewal of liver CSCs. Thus, *lncHand2* and *HAND2* exert separate roles in the regulation of liver oncogenesis. Intriguingly, human ortholog *HAND2-AS1* is highly expressed in liver CSCs, but almost undetectable in liver cirrhosis samples and healthy liver tissues. What triggers high expression of *HAND2-AS1* in liver CSCs still needs to be further investigated.

The BMP signaling plays a pivotal role in the regulation of self-renewal and differentiation of stem cells (Genander et al, 2014; Jain et al, 2015; Munera et al, 2017). Activation of BMP signaling is mediated by ligand-induced heterotetrameric complex formation. These complexes encompass two type I and two type II serine–threonine kinase receptors on target cell membranes, and the BMP type I receptors exert indispensable roles in transducing BMP signaling. The BMP type I receptors can be classified into two groups: the BMP type-IA receptor (BMPR-IA; also known as ALK3) and BMP type-IB

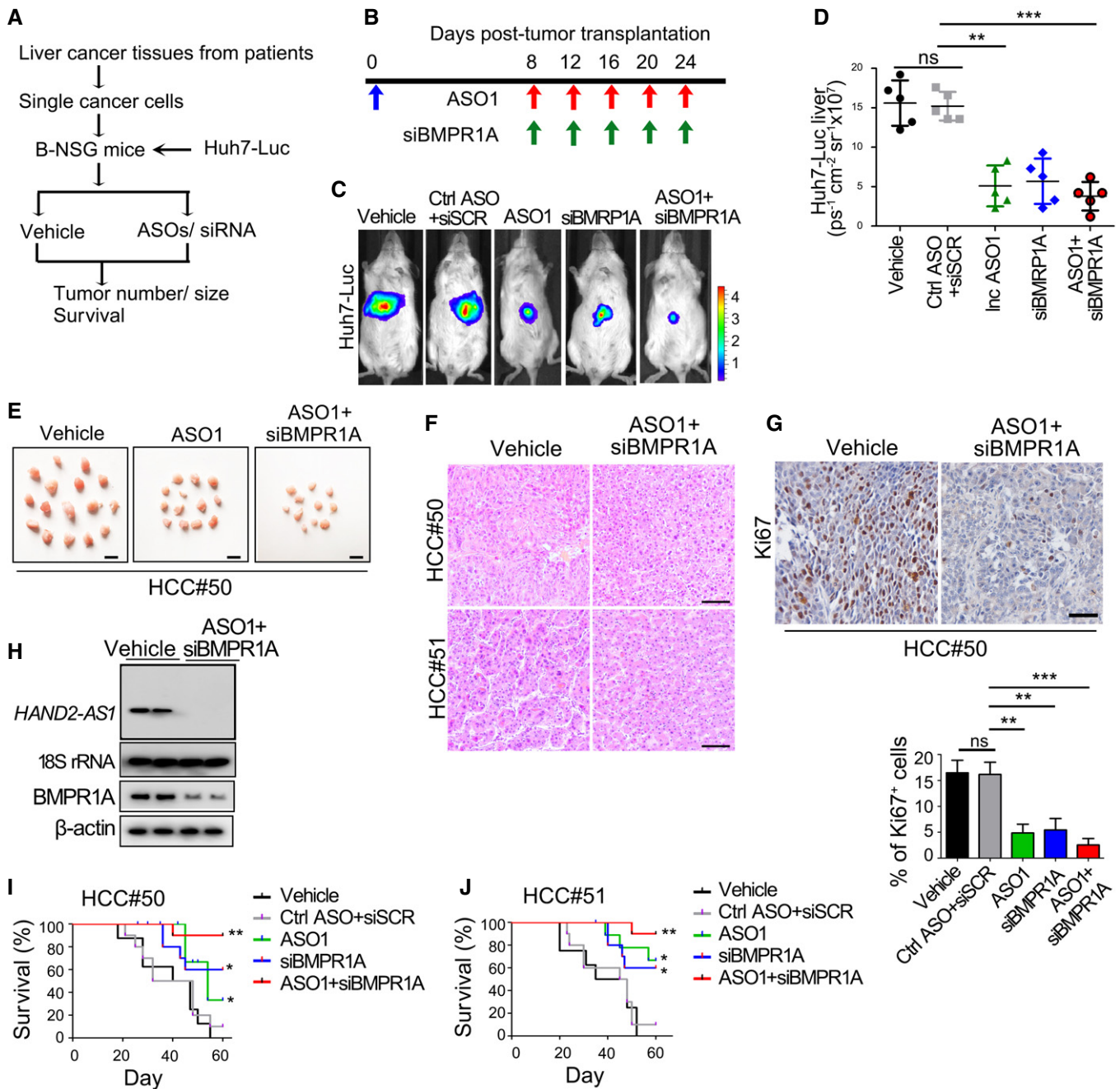


Figure 6.

receptor (BMPR-IB; also known as ALK6) group, and the serine/threonine-protein kinase receptor R3 (SKR3, also known as ALK1) and activin receptor type-1 (ACTR-I; also known as ALK2) group (Morrell *et al*, 2016). Of note, these receptors are restrictedly expressed on various target cells. Moreover, each BMP type I receptor has a distinct role during embryogenesis in mammals. For instance, knockout of *Bmpr1a* or *Acrv1* causes embryonic lethality at different stages of gastrulation (Mishina *et al*, 1995), whereas knockout of *Bmpr1b* has no lethal influence during embryogenesis (Beppu *et al*, 2000). It has been reported that aberrant activation of the BMP signaling is implicated in the pathogenesis of pediatric

acute leukemia (Crispino & Le Beau, 2012) and lung cancer (Wang *et al*, 2015b). However, how BMP signaling is activated and regulates liver cancer development remains largely unknown. We revealed that *HAND2-AS1* can activate the BMP signaling to sustain the self-renewal of liver CSCs. We showed that BMPR1A, as a direct binding target of *HAND2-AS1*, is highly expressed in HCC tumors, and it is also an ideal prognosis predictor for liver cancers. BMPR1A depletion impairs sphere formation and tumor-initiating capacity. *Bmpr1a* deletion in mice reduces liver tumor formation capacity after treated with DEN. Moreover, administration of siRNAs against BMPR1A can inhibit tumor growth and tumor numbers compared to

Figure 6. ASOs of *HAND2-AS1* and siRNAs against *BMPR1A* have synergistic anti-tumor effects on humanized HCC models.

- A Schematic representation of the experimental workflow. Patient-derived HCC cells or Huh7-Luc cell lines were orthotopically transplanted into livers of B-NSG mice. Then, mice were treated with scramble RNAs, ASOs for *HAND2-AS1*, and/or combined with siRNAs for *BMPR1A*.
- B Illustration of ASO/siRNA treatment timeline.
- C Representative whole-body imaging of Huh7-Luc cells in different groups. Mice treated with scramble ASOs and/or siRNAs obtained similar results to vehicle treatment. $n \geq 5$ mice in each group.
- D Quantification of tumor numbers treated with ASOs and/or siRNAs after Huh7-Luc tumor cells orthotopically implanted to B-NSG mice. Calculated data are shown as means \pm SD ($n = 5$).
- E Tumors were excised from livers of PDX liver cancer models. Scale bar, 0.5 cm.
- F Representative H&E staining in liver sections from tumor-bearing mice treated with ASO1 and siBMPR1A in orthotopic transplants of tumors from HCC#50 and HCC#51. Scale bar, 100 μ m.
- G Representative immunohistological staining with Ki67 antibody of tumor-bearing mice treated with ASO1 and siBMPR1A. Scale bar, 100 μ m. Lower panel: quantitation of Ki67-positive cells in different groups. Data are shown as means \pm SD ($n = 5$ per group).
- H Northern blotting of *HAND2-AS1* and immunoblotting of *BMPR1A* in tumors from PDX HCC#50 after treatment.
- I, J Kaplan–Meier survival analysis of B-NSG mice orthotopically transplanted with PDXs HCC#50 (I) and HCC#51 (J). Treatment with ASO1 combined siBMPR1A causes synergistic therapeutic effect than each treatment alone ($n = 10$ per group). *P*-value for Kaplan–Meier curves was determined using a Mantel–Cox log-rank test.
- Data information: ***P* < 0.01 and ****P* < 0.001 by two-tailed Student's *t*-test unless indicated otherwise.

vehicle-treated group. Our findings suggest that *BMPR1A*-mediated BMP signaling plays a critical role in the self-renewal maintenance of liver CSC and liver tumorigenesis.

Several studies have identified some lncRNAs as cancer biomarkers. For example, *PCA3* serves as a biomarker for prostate cancer diagnosis (Vlaeminck-Guillem *et al*, 2008; Hessels & Schalken, 2009), the first diagnostic lncRNA approved by FDA. Recent large-scale transcriptome sequencing approaches have identified huge amounts of lncRNAs (Mondal *et al*, 2018; Wang *et al*, 2018b), suggesting more lncRNAs may play critical roles in the tumorigenesis and will be used as ideal biomarkers for cancer diagnosis and potential drug targets. Therapies designed to target cancer-related lncRNAs are also under intensive investigation. ASO therapy has been applied in neural diseases in non-human primates and human clinical trials through intrathecal administration, without serious adverse reactions (Kordasiewicz *et al*, 2012; Miller *et al*, 2013). In this study, we showed that ASOs of *HAND2-AS1* combined with siRNAs against *BMPR1A* can dramatically reduce tumor growth and consequently improve overall survival in PDX hepatocellular carcinoma models. In addition, only administration of ASOs against *HAND2-AS1* still has potent anti-tumor activity, suggesting that targeting lncRNAs by ASOs could be potential therapeutic targets for hepatocellular carcinoma. However, how to effectively deliver RNA-based oligonucleotides into tumors and keep long-lasting efficacy against tumors still requires to be intensively investigated in the tumor biology field. In summary, *HAND2-AS1* promotes the self-renewal of liver CSCs and drives liver tumorigenesis, which may be a potential biomarker for liver cancer diagnosis and target for HCC therapy.

Materials and Methods

Antibodies and reagents

Antibodies used were as follows: Anti-Ki67 (ab15580), anti-INO80 (ab105451), anti-IES2 (ab175117), anti-HAND2 (ab10131), anti-*BMPR1A* (ab38560), and anti-Digoxin (ab51949) antibodies were purchased from Abcam. Anti-RUVBL2 (10195-1-AP), anti-RUVBL1 (10210-2-AP), anti-AMIDA (10097-2-AP), anti-ARP4 (18374-1-AP), anti-ARP5 (21505-1-AP), anti-BAF53A (10341-1-AP), anti-IES6

(24793-1-AP), anti-YY1 (2E11C5), and anti-GFP (1E10H7) were from Proteintech. Anti-phospho-Smad1/5 (Ser463/465) (41D10) was from Cell Signaling Technology. Anti- β -actin was from Sigma-Aldrich. Recombinant INO80 was from Abnova. Donkey anti-rabbit, anti-mouse, anti-goat IgG secondary antibodies conjugated with Alexa-594, Alexa-488, and Alexa-647-conjugated secondary antibodies were purchased from Invitrogen. HRP-conjugated secondary antibodies were from Santa Cruz. Tyramide signal amplification for fluorescence *in situ* hybridization and immunohistochemistry kits were from PerkinElmer. DAPI, DEN, and D-Luciferin were from Sigma-Aldrich.

Cell lines and oncosphere formation assay

Human hepatocellular carcinoma (HCC) cell lines Hep3B, Huh7, and PLC/PRF/5 were maintained in DMEM supplemented with 10% fetal bovine serum (FBS), 100 μ g/ml penicillin G, and 100 U/ml streptomycin (Invitrogen, NY, USA). Cells were seeded on ultra-low attachment culture dishes (Corning) in serum-free medium. DMEM/F12 serum-free medium (Invitrogen) contained 2 mM L-glutamine, 1% sodium pyruvate (Invitrogen), 100 μ g/ml penicillin G, and 100 U/ml streptomycin supplemented with 20 ng/ml epithelial growth factor (Invitrogen), 10 ng/ml fibroblast growth factor-2 (Invitrogen), N2 (Invitrogen), and B27 (Invitrogen).

Animals

LncHand2^{flox/flox} and *Ino80*^{flox/flox} mice were generated using CRISPR/Cas9 approaches as previously described (Zhu *et al*, 2014; Wang *et al*, 2018a). All mouse genotypes were verified by DNA sequencing. Alb-Cre mice were from Shanghai Model Organisms Center, Inc (China). Animals were killed when sick or when they developed tumors larger than 15 mm in their greater diameter or ulcerated lesions. Mouse experiments were approved by the Institutional Animal Care and Use Committees at the Institute of Biophysics, Chinese Academy of Sciences. We used littermates with the same age (8–12 weeks old) and gender for each group. We excluded the mice 5 g thinner than other littermates before any treatment or analysis. We did not use randomization in our animal studies. We were not blinded to the group in our animal studies.

Gene knockout by CRISPR/Cas9-mediated genome editing *in vivo*

Bmpr1a gene deletion mice were established by CRISPR/Cas9-mediated genome editing *in vivo* as described (Platt *et al*, 2014). Briefly, we cloned sgRNA into adeno-associated virus (AAV) vector (Addgene #60231) and transfected into 293T cells along with pHelper vector (Biovector NTCC Inc) and pAnc80L65 vector (Addgene #68837) for 72 h. Then, transfected cells were lysed by repeated unfreezing and AAV was purified for splenic injection into CRISPR/Cas9 knockin mice (Jackson Laboratory, Stock no: 024857), and gene deletion efficiency was examined by Western blot 1 week post-injection. sgRNA sequences used for this study were listed in Appendix Table S1.

Patients and sample collection

Primary HCC patients with hepatectomy were recruited in this study. Pathological diagnosis was made according to the histology of tumor specimens or biopsy and examined by experienced pathologists. Liver cirrhosis and normal livers were used as controls. The diagnosis of cirrhosis was made according to histological findings in liver explants or CT/MRI results. All tissue samples were obtained from consenting patients and approved by the Institutional Review Board of the Institute of Biophysics, Chinese Academy of Sciences. All specimens were obtained from the partial hepatectomy series at the Department of Hepatobiliary Surgery, PLA General Hospital (Beijing, China). The clinical data for the above patients are summarized in Appendix Table S2.

Patient-derived xenograft (PDX) liver cancer model and RNA treatment

Patient-derived samples were obtained from patients who had given informed consent. Human hepatocytes were isolated by a two-step collagenase perfusion method with slight modification. Briefly, the liver was perfused at 5 ml/min with EGTA buffer at 37°C for 5 min via the portal vein. Subsequently, the liver was further perfused using collagenase and dispase (collagenase IV dispase 4 mg/ml; Invitrogen) at 37°C for 1 h. The liver was then dissociated in suspension buffer and filtered with 100 µm cell strainer. Hepatocytes were collected by centrifugation at 50 g for 2 min. Passage-1 PDXs were then orthotopically transplanted into B-NSG mice via injection with 2×10^5 hepatocytes. ASOs (30 mg/kg) and/or siRNAs (30 mg/kg) were intraperitoneally injected on days 8, 12, 16, 20, and 24. Tumor growth was detected after 28 days.

Microarray analysis

For liver CSCs and CSCs sorting, cocktail PE-conjugated anti-human CD133 and FITC-conjugated anti-human CD13 antibodies were incubated with HCC primary cells, followed by sorting with FACS Aria III (BD Immunocytometry Systems, San Jose, CA, USA). Cells were collected for total RNA extraction with Trizol reagent. Samples were analyzed with Agilent lncRNA microarray.

Genome-wide expression profiling assay of cells with *HAND2-AS1* and INO80 being knocked down by shRNA as well as scramble control was carried out in custom-designed microarray (Agilent Platform). Feature extraction software was used to extract all features of

the data from the scanned images, followed by background subtraction and quality control. Quantile normalization was carried out on the whole set of probes. Expression values were log₂-scale transformed, and then, probes for transcripts were collapsed down to gene level.

In vitro coding potential assay

The potential ORF sequences of *HAND2-AS1* and GFP were cloned in frame into pcDNA3.1(+) with double enzyme digestion reactions. GFP antibody was used to detect whether the predicted *HAND2-AS1* ORF sequence could be translated as a fusion protein with GFP.

RNA fluorescence *in situ* hybridization (FISH)

Fluorescence-conjugated *HAND2-AS1* probes were used for RNA FISH. RNA FISH was performed as previously described. Hybridization was carried out using DNA probe sets (Biosearch Technologies) according to the protocol of Biosearch Technologies. Oncosphere and control cells were observed with a FV1000 confocal laser microscopy (Olympus).

RNA pulldown and mass spectrometry (MS) assay

RNA pulldown was performed as described (Klattenhoff *et al*, 2013). *In vitro* biotin-labeled RNAs (*HAND2-AS1*, its antisense RNA, and an intron control RNAs of *HAND2-AS1*) were transcribed with the biotin RNA labeling mix (Roche) and T7 RNA polymerase (Roche) treated with RNase-free DNase I (Promega) and purified with RNeasy Mini Kit (QIAGEN). Biotinylated RNA was incubated with HCC oncosphere cell nuclear extracts, and pulldown proteins were run on SDS-PAGE gels, followed by mass spectrometry.

CRISPR-Cas9 knockout system in HCC cell lines

HAND2-AS1 Huh7, Hep3B, and Huh7-Luc cells were established with a CRISPR-Cas9 system (Zhu *et al*, 2016a). For *HAND2-AS1* rescue, *HAND2-AS1*-overexpressing lentivirus was co-infected, and this was followed by puromycin and GFP sorting.

RNA-EMSA assay

EMSA experiments were performed using a LightShift Chemiluminescent RNA EMSA Kit (Thermo Scientific).

Chromatin isolation by RNA purification-sequencing (ChIRP-seq) and bioinformatics analysis

Chromatin isolation by RNA purification (ChIRP) was performed as described previously (Chu *et al*, 2012). In brief, human liver cells were cross-linked using glutaraldehyde. After glycine quenching, the nuclear lysate was sonicated for 25–30 cycles, 30 s on 30 s off at 4°C, with BioRuptor twin sonicator (Diagenode). Ten *HAND2-AS1* and eight LacZ pulldown probes with BiotinTEG were designed by Biosearch Technologies and allowed to hybridize overnight with sonicated chromatin at 37°C (100 pmol probe per 1 ml chromatin).

After hybridization, C1 Dynabeads (Life Technologies) were added and incubated for 30 min. For protein elution for mass spectrometry analysis, washed beads were resuspended in 3 × original volume of DNase buffer (100 mM NaCl and 0.1% NP-40), and protein was eluted with a cocktail of 50 mM triethylammonium bicarbonate, 12 mM sodium lauryl sarcosine, and 0.5% sodium deoxycholate supplemented with 100 µg/ml RNase A (Sigma-Aldrich) and 0.1 U/µl RNase H (Epicentre), and 100 U/ml DNase I (Invitrogen). For RNA isolation, beads were resuspended in proteinase K buffer [100 mM NaCl, 10 mM Tris-Cl, pH 7.0, 1 mM EDTA, 0.5% SDS, 5% by volume proteinase K (AM2546, Ambion) 20 mg/ml] and incubated at 50°C followed by Trizol isolation and DNase treatment. We repeated the ChIRP-seq experiments for three times.

The paired-end sequencing reads were mapped to the human genome (hg19) sequence using bowtie2, and the duplicate reads were subsequently removed by Picard with default parameters. The enriched peaks were called by MACS2. For each peak, we filtered for peaks that share the same shape from the three independent experiments. Only peaks with high correlation of the raw data profile and high coverage across the peak were accepted. Peaks from all the samples were intersecting peaks from three replicative ChIRP-seq experiments. For *HAND2-AS1* ChIRP-seq sample, thresholds of average coverage > 1.5, Pearson correlation > 0.3, and fold enrichment against input > 2 were applied to filter MACS predicted peaks. Regions overlapping any enriched peaks called by the negative controls (LacZ probes) were discarded, and only the regions which share no sequence similarity with the LacZ probes were kept for further analysis.

IVIS *in vivo* imaging

Detection of luciferase activity was performed in an IVIS-100 imaging system. Five minutes before the procedure, mice were injected intraperitoneally with D-luciferin, bioluminescence substrate (Sigma) according to the manufacturer's instructions. Living Image 4.3 software (PerkinElmer) was used for analysis of the images after acquisition.

Immunohistochemistry

Tumor samples were fixed in 4% formaldehyde for 24 h at room temperature, moved into 70% ethanol for 12 h, and then embedded in paraffin. After cutting (Leica RM2235) and baking at 60°C for 20 min for de-paraffinization, slides were treated for antigen unmasking. For immunohistochemical staining, endogenous peroxidases were inactivated by 3% hydrogen peroxide at room temperature (RT) for 15 min. Non-specific signals were blocked with 5% BSA and 5% goat serum for 1 h. Tissues were stained with primary antibodies for 12 h at 4°C. After washing with PBS-T, tissues were stained with secondary antibodies against mouse, rabbit, or goat for 1 h, RT. For immunofluorescence, secondary antibodies conjugated to Alexa594 (Molecular Probes) were used. Images were captured with Olympus confocal microscope.

Statistical analysis

Data were analyzed with a double-sided Student's *t*-test using the SPSS 13.0 software and GraphPad Prism 6. Tumorigenic cell

frequency was calculated based on extreme limiting dilution analysis (ELDA) (<http://bioinf.wehi.edu.au/software/elda/>). *P*-values less than 0.05 were considered statistically significant. For other methods, see the Appendix.

Data availability

Microarray data and ChIRP-seq data have been deposited in the NCBI GEO under accession numbers GSE122420 (<https://www.ncbi.nlm.nih.gov/geo/query/acc.cgi?acc=GSE122420>) and GSE126123 (<https://www.ncbi.nlm.nih.gov/geo/query/acc.cgi?acc=GSE126123>).

Expanded View for this article is available online.

Acknowledgements

We thank Drs. Yihui Xu, Xiang Shi, Xiaoxiao Zhu, Dongdong Fan, Xing Gao, Meng Wan, Shu Meng, Jing Cheng, Zhensheng Xie, and Yan Teng for technical support. We thank J. Li (Cnkingbio Company Ltd, Beijing, China) for technical support. This work was supported by Strategic Priority Research Programs of the Chinese Academy of Sciences (XDA19050301, XDA12020219, and XDB19030203), the National Natural Science Foundation of China (91640203, 31530093, 81872413, 81672897, 81602247, 81572433, 81772646, and 31601189), Beijing Natural Science Foundation (7181006, 7162125), and Youth Innovation Promotion Association of CAS to Y.W.

Author contributions

YW designed and performed experiments, analyzed data, and wrote the paper; PZ, JL, and Jing Wang constructed plasmids, performed experiments, and analyzed data; ZL, LH, and WR provided clinical specimens and analyzed data. WW performed bioinformatics analysis of microarray and ChIRP-seq data. XS performed some bioinformatics analysis. YD, BY, DW, and Jianyi Wang performed some experiments. RC and YT initiated the study; ZF initiated the study, organized, designed, and wrote the paper.

Conflict of interest

The authors declare that they have no conflict of interest.

References

- Albert I, Mavrich TN, Tomsho LP, Qi J, Zanton SJ, Schuster SC, Pugh BF (2007) Translational and rotational settings of H2A.Z nucleosomes across the *Saccharomyces cerevisiae* genome. *Nature* 446: 572–576
- Andersen P, Tampakakis E, Jimenez DV, Kannan S, Miyamoto M, Shin HK, Saberi A, Murphy S, Sulistio E, Chelko SP *et al* (2018) Precardiac organoids form two heart fields via Bmp/Wnt signaling. *Nat Commun* 9: 3140
- Ayala R, Willhoft O, Aramayo RJ, Wilkinson M, McCormack EA, Ocloo L, Wigley DB, Zhang X (2018) Structure and regulation of the human INO80-nucleosome complex. *Nature* 556: 391–395
- Batista PJ, Chang HY (2013) Long noncoding RNAs: cellular address codes in development and disease. *Cell* 152: 1298–1307
- Beppu H, Kawabata M, Hamamoto T, Chytil A, Minowa O, Noda T, Miyazono K (2000) BMP type II receptor is required for gastrulation and early development of mouse embryos. *Dev Biol* 221: 249–258
- Boumahdi S, Driessens G, Lapouge G, Rorive S, Nassar D, Le Mercier M, Delatte B, Caauwe A, Lenglez S, Nkusi E *et al* (2014) SOX2 controls tumour

- initiation and cancer stem-cell functions in squamous-cell carcinoma. *Nature* 511: 246–250
- Chu C, Quinn J, Chang HY (2012) Chromatin isolation by RNA purification (ChIRP). *J Vis Exp* 61: 3912
- Chu C, Zhang QC, da Rocha ST, Flynn RA, Bharadwaj M, Calabrese JM, Magnuson T, Heard E, Chang HY (2015) Systematic discovery of Xist RNA binding proteins. *Cell* 161: 404–416
- Crispino JD, Le Beau MM (2012) BMP meets AML: induction of BMP signaling by a novel fusion gene promotes pediatric acute leukemia. *Cancer Cell* 22: 567–568
- Eustermann S, Schall K, Kostrewa D, Lakomek K, Strauss M, Moldt M, Hopfner KP (2018) Structural basis for ATP-dependent chromatin remodelling by the INO80 complex. *Nature* 556: 386–390
- Fatica A, Bozzoni I (2014) Long non-coding RNAs: new players in cell differentiation and development. *Nat Rev Genet* 15: 7–21
- Flynn RA, Chang HY (2014) Long noncoding RNAs in cell-fate programming and reprogramming. *Cell Stem Cell* 14: 752–761
- Genander M, Cook PJ, Ramskold D, Keyes BE, Mertz AF, Sandberg R, Fuchs E (2014) BMP signaling and its pSMAD1/5 target genes differentially regulate hair follicle stem cell lineages. *Cell Stem Cell* 15: 619–633
- Hessels D, Schalken JA (2009) The use of PCA3 in the diagnosis of prostate cancer. *Nat Rev Urol* 6: 255–261
- Hosono Y, Niknafs YS, Prensner JR, Iyer MK, Dhanasekaran SM, Mehra R, Pitchiaya S, Tien J, Escara-Wilke J, Poliakov A et al (2017) Oncogenic role of THOR, a conserved cancer/testis long non-coding RNA. *Cell* 171: 1559–1572 e20
- Jain R, Li D, Gupta M, Manderfield LJ, Izkovits JL, Wang Q, Liu F, Liu Y, Poleshko A, Padmanabhan A et al (2015) HEART DEVELOPMENT. Integration of Bmp and Wnt signaling by Hopx specifies commitment of cardiomyoblasts. *Science* 348: aaa6071
- Ji J, Shi J, Budhu A, Yu Z, Forgues M, Roessler S, Ambros S, Chen Y, Meltzer PS, Croce CM et al (2009) MicroRNA expression, survival, and response to interferon in liver cancer. *N Engl J Med* 361: 1437–1447
- Kaiser J (2015) The cancer stem cell gamble. *Science* 347: 226–229
- Kirmizitas A, Meiklejohn S, Ciau-Uitz A, Stephenson R, Patient R (2017) Dissecting BMP signaling input into the gene regulatory networks driving specification of the blood stem cell lineage. *Proc Natl Acad Sci USA* 114: 5814–5821
- Klattenhoff CA, Scheuermann JC, Surface LE, Bradley RK, Fields PA, Steinhilber ML, Ding H, Butty VL, Torrey L, Haas S et al (2013) Braveheart, a long noncoding RNA required for cardiovascular lineage commitment. *Cell* 152: 570–583
- Kopp F, Mendell JT (2018) Functional classification and experimental dissection of long noncoding RNAs. *Cell* 172: 393–407
- Kordasiewicz HB, Stanek LM, Wancewicz EV, Mazur C, McAlonis MM, Pytel KA, Artates JW, Weiss A, Cheng SH, Shihabuddin LS et al (2012) Sustained therapeutic reversal of Huntington's disease by transient repression of huntingtin synthesis. *Neuron* 74: 1031–1044
- Krientein N, Wal M, Watanabe S, Park B, Peterson CL, Pugh BF, Korber P (2016) Genomic nucleosome organization reconstituted with pure proteins. *Cell* 167: 709–721 e12
- Lau E (2014) Non-coding RNA: zooming in on lncRNA functions. *Nat Rev Genet* 15: 574–575
- Leucci E, Vendramin R, Spinazzi M, Laurette P, Fiers M, Wouters J, Radaelli E, Eyckerman S, Leonelli C, Vanderheyden K et al (2016) Melanoma addiction to the long non-coding RNA SAMMSON. *Nature* 531: 518–522
- Luo S, Lu JY, Liu L, Yin Y, Chen C, Han X, Wu B, Xu R, Liu W, Yan P et al (2016) Divergent lncRNAs regulate gene expression and lineage differentiation in pluripotent cells. *Cell Stem Cell* 18: 637–652
- Marquardt JU, Andersen JB, Thorgeirsson SS (2015) Functional and genetic deconstruction of the cellular origin in liver cancer. *Nat Rev Cancer* 15: 653–667
- Matsui M, Corey DR (2017) Non-coding RNAs as drug targets. *Nat Rev Drug Discov* 16: 167–179
- Meacham CE, Morrison SJ (2013) Tumour heterogeneity and cancer cell plasticity. *Nature* 501: 328–337
- Meng L, Ward AJ, Chun S, Bennett CF, Beaudet AL, Rigo F (2015) Towards a therapy for Angelman syndrome by targeting a long non-coding RNA. *Nature* 518: 409–412
- Miller TM, Pestronk A, David W, Rothstein J, Simpson E, Appel SH, Andres PL, Mahoney K, Allred P, Alexander K et al (2013) An antisense oligonucleotide against SOD1 delivered intrathecally for patients with SOD1 familial amyotrophic lateral sclerosis: a phase 1, randomised, first-in-man study. *Lancet Neurol* 12: 435–442
- Mishina Y, Suzuki A, Ueno N, Behringer RR (1995) Bmpr encodes a type I bone morphogenetic protein receptor that is essential for gastrulation during mouse embryogenesis. *Genes Dev* 9: 3027–3037
- Mondal T, Juvvuna PK, Kirkeby A, Mitra S, Kosalaj ST, Traxler L, Hertwig F, Wernig-Zorc S, Miranda C, Deland L et al (2018) Sense-antisense lncRNA pair encoded by locus 6p22.3 determines neuroblastoma susceptibility via the USP36-CHD7-SOX9 regulatory axis. *Cancer Cell* 33: 417–434 e7
- Morrell NW, Bloch DB, ten Dijke P, Goumans MJ, Hata A, Smith J, Yu PB, Bloch KD (2016) Targeting BMP signalling in cardiovascular disease and anaemia. *Nat Rev Cardiol* 13: 106–120
- Munera JO, Sundaram N, Rankin SA, Hill D, Watson C, Mahe M, Vallance JE, Shroyer NF, Sinagoga KL, Zarzoso-Lacoste A et al (2017) Differentiation of human pluripotent stem cells into colonic organoids via transient activation of BMP signaling. *Cell Stem Cell* 21: 51–64 e6
- Papamichos-Chronakis M, Watanabe S, Rando OJ, Peterson CL (2011) Global regulation of H2A.Z localization by the INO80 chromatin-remodeling enzyme is essential for genome integrity. *Cell* 144: 200–213
- Platt RJ, Chen SD, Zhou Y, Yim MJ, Swiech L, Kempton HR, Dahlman JE, Parnas O, Eisenhaure TM, Jovanovic M et al (2014) CRISPR-Cas9 knockin mice for genome editing and cancer modeling. *Cell* 159: 440–455
- Sallam T, Jones MC, Gilliland T, Zhang L, Wu X, Eskin A, Sandhu J, Casero D, Vallim TQ, Hong C et al (2016) Feedback modulation of cholesterol metabolism by the lipid-responsive non-coding RNA LeXis. *Nature* 534: 124–128
- Ulitksy I, Bartel DP (2013) lincRNAs: genomics, evolution, and mechanisms. *Cell* 154: 26–46
- Visvader JE (2011) Cells of origin in cancer. *Nature* 469: 314–322
- Vlaeminck-Guillem V, Ruffion A, Andre J (2008) Value of urinary PCA3 test for prostate cancer diagnosis. *Prog Urol* 18: 259–265
- Wang L, Du Y, Ward JM, Shimbo T, Lackford B, Zheng X, Miao YL, Zhou B, Han L, Fargo DC et al (2014) INO80 facilitates pluripotency gene activation in embryonic stem cell self-renewal, reprogramming, and blastocyst development. *Cell Stem Cell* 14: 575–591
- Wang Y, He L, Du Y, Zhu P, Huang G, Luo J, Yan X, Ye B, Li C, Xia P et al (2015a) The long noncoding RNA lncTCF7 promotes self-renewal of human liver cancer stem cells through activation of Wnt signaling. *Cell Stem Cell* 16: 413–425

- Wang Z, Shen Z, Li Z, Duan J, Fu S, Liu Z, Bai H, Zhang Z, Zhao J, Wang X et al (2015b) Activation of the BMP-BMPR pathway conferred resistance to EGFR-TKIs in lung squamous cell carcinoma patients with EGFR mutations. *Proc Natl Acad Sci USA* 112: 9990–9995
- Wang Y, Zhu P, Wang J, Zhu X, Luo J, Meng S, Wu J, Ye B, He L, Du Y et al (2018a) Long noncoding RNA LncHand2 promotes liver repopulation via c-Met signaling. *J Hepatol* 69: 861–872
- Wang Z, Yang B, Zhang M, Guo W, Wu Z, Wang Y, Jia L, Li S, Cancer Genome Atlas Research Network, Xie W et al (2018b) lncRNA epigenetic landscape analysis identifies EPIC1 as an oncogenic lncRNA that interacts with MYC and promotes cell-cycle progression in cancer. *Cancer Cell* 33: 706–720 e9
- Xing YH, Yao RW, Zhang Y, Guo CJ, Jiang S, Xu G, Dong R, Yang L, Chen LL (2017) SLERT regulates DDX21 rings associated with Pol I transcription. *Cell* 169: 664–678 e16
- Yang Y, Chen L, Gu J, Zhang H, Yuan J, Lian Q, Lv G, Wang S, Wu Y, Yang YT et al (2017) Recurrently deregulated lncRNAs in hepatocellular carcinoma. *Nat Commun* 8: 14421
- Yang X, Wang CC, Lee WYW, Trovik J, Chung TKH, Kwong J (2018) Long non-coding RNA HAND2-AS1 inhibits invasion and metastasis in endometrioid endometrial carcinoma through inactivating neuromedin U. *Cancer Lett* 413: 23–34
- Zhu X, Xu Y, Yu S, Lu L, Ding M, Cheng J, Song G, Gao X, Yao L, Fan D et al (2014) An efficient genotyping method for genome-modified animals and human cells generated with CRISPR/Cas9 system. *Sci Rep* 4: 6420
- Zhu P, Wang Y, He L, Huang G, Du Y, Zhang G, Yan X, Xia P, Ye B, Wang S et al (2015) ZIC2-dependent OCT4 activation drives self-renewal of human liver cancer stem cells. *J Clin Invest* 125: 3795–3808
- Zhu P, Wang Y, Huang G, Ye B, Liu B, Wu J, Du Y, He L, Fan Z (2016a) lnc-beta-Catm elicits EZH2-dependent beta-catenin stabilization and sustains liver CSC self-renewal. *Nat Struct Mol Biol* 23: 631–639
- Zhu P, Wang Y, Wu J, Huang G, Liu B, Ye B, Du Y, Gao G, Tian Y, He L et al (2016b) lncBRM initiates YAP1 signalling activation to drive self-renewal of liver cancer stem cells. *Nat Commun* 7: 13608